

TRANSONIC FLUTTER, SHOCKS, AND PARAMETER EFFECTS

T. K. Pradeepa, Kartik Venkatraman

Department of Aerospace Engineering, Indian Institute of Science, Bangalore.

pradeep@aero.iisc.ernet.in; kartik@aero.iisc.ernet.in

Keywords: *Transonic flow, Transonic flutter, Limit cycle, Static divergence, Energy transfer*

Abstract

There is a drop in the flutter boundary of an aeroelastic system placed in a transonic flow due to compressibility effects and is known as the transonic dip. Viscous effects can shift the location of the shock and depending on the shock strength the boundary layer may separate leading to changes in the flutter speed. An unsteady Euler flow solver coupled with the structural dynamic equations is used to understand the effect of shock on the transonic dip. The effect of various system parameters such as mass ratio, location of the center of mass, position of the elastic axis, ratio of uncoupled natural frequencies in heave and pitch are also studied. Steady turbulent flow results are presented to demonstrate the effect of viscosity on the location and strength of the shock.

1 Introduction

Flutter is a dynamic aeroelastic instability wherein at a particular flow speed a self-sustained oscillation of the structure persists. A further increase in flow speed leads to oscillations of the structure with increasing amplitude. Flutter occurs because the wings can absorb energy from the airstream. In classical bending-torsion flutter, the phase difference between the bending and the torsional motions lead to flutter with no appearance of separation nor strong shocks [1]. The energy absorbed by an airfoil in pitching alone can become positive provided there is a phase differ-

ence between the airfoil pitching motion and the aerodynamic pitching moment. This phase difference is due to the shed vortices and the flow compressibility [2]. The transonic flutter boundary drops because of this pronounced compressibility effect, and this is known as the transonic dip. Viscous effects can shift the location of the shock and also depending upon the shock strength, the boundary layer may separate leading to changes in the flutter speed.

Linearized aerodynamic theory cannot predict transonic flutter instability due to the presence of part-chord shock. Also, the motion of the shock is not in phase with the airfoil motion. To predict this behavior, the exact location and strength of the shock needs to be computed. At the same time, the phase difference between the motion of the airfoil and the aerodynamic forces including the effect of shed vortices and shock motion should be captured. For this it is required to solve the unsteady Navier-Stokes equations coupled with the structural dynamic governing equations.

Ashley [3] gave a qualitative estimation of transonic flutter for a lifting surface. The importance of the influence of shock and other system parameters on flutter was highlighted. The unsteady air load was expressed as the sum of the load due to linearized theory and a shock force doublet centered at the steady shock location. The role of shocks on flexure-torsion flutter was explained by calculating the energy transferred to the structure due to the shock motion. Besides, the effect of parameters such as mass ratio, loca-

tion of center of mass, and the ratio of heave and pitch spring stiffness were also described. Isogai [2] studied the effect of various system parameters and the effect of shock on the flutter characteristics of an airfoil in the transonic regime. The system parameters considered were the mass ratio, stiffness of the spring in pitch and heave, location of the elastic axis and the position of mass center. The unsteady aerodynamic calculations used a linearized subsonic theory. Later Isogai [4] took up the same study with the unsteady air loads being calculated using the transonic small perturbation theory. The assumption that there is no entropy production and vorticity generation across the shock in the potential flow equation make these analysis limited in scope. Though Bendiksen [5] showed energy transfer by aerodynamic forces into the wing, this was demonstrated only in order to determine the contributions from different regions of the flow. The location of the shock and its dynamics were used to explain the transonic dip phenomenon.

In the present work a quantitative study of the energy transfer from the fluid to the structure due to the shock motion is made which helps in understanding the transonic dip in a better way. In the present work an unsteady Euler flow solver on a moving grid using the algorithm with central space discretization is carried out with dissipative terms added to eliminate unphysical oscillations in the solution [6]. An explicit Runge-Kutta time integration is done for time marching. The aeroelastic equations are solved using a linear acceleration technique. The contribution of the shock motion to the energy input into the structure is computed. An attempt to understand the transonic dip through energy concepts is made. The flutter behavior for variation in the structural parameters is also studied. The effect of viscosity in shifting the shock location is presented.

2 Mathematical formulation

2.1 Flow solver

The unsteady Euler equations in integral form for a two dimensional moving mesh can be written as

$$\frac{\partial}{\partial t} \iint_{\Omega} W dx dy + \int_{\partial\Omega} f dy - g dx = 0. \quad (1)$$

Here

$$f = \begin{pmatrix} \rho(u - x_{\tau}) \\ \rho(u - x_{\tau})u + p \\ \rho(u - x_{\tau})v \\ \rho E(u - x_{\tau}) + pu \end{pmatrix}, \quad g = \begin{pmatrix} \rho(v - y_{\tau}) \\ \rho(v - y_{\tau})u \\ \rho(v - y_{\tau})v + p \\ \rho E(v - y_{\tau}) + pv \end{pmatrix}.$$

W is a vector of conserved variables, f and g are the flux vectors in the x and y directions respectively, ρ is the density. u and v are velocities in the x and y directions respectively. x_{τ} and y_{τ} are velocities of the moving mesh in the x and y directions respectively. p is the pressure and E is the total internal energy of the fluid. From the equation of state for a perfect gas, the total specific internal energy is

$$E = \frac{1}{\gamma - 1} \frac{p}{\rho} + \frac{1}{2} (u^2 + v^2).$$

Finite volume discretization of Equation (1) for each cell with cell centered scheme yields

$$\frac{d}{dt} (S_{ij} W_{ij}) + Q_{ij} = 0, \quad (2)$$

where

$$Q_{ij} = \sum_{k=1}^4 \Delta y_k f_k - \Delta x_k g_k.$$

Here S_{ij} is the area of the cell i, j and Δy_k and Δx_k are the length of the face k in y and x directions of the quadrilateral cell. As we are solving the weak form of the governing equations, unphysical solutions such as oscillations near the shock are part of the solution. In order to get a physically correct solution, numerical dissipation is added as

$$\frac{d}{dt} (S_{ij} W_{ij}) + Q_{ij} - D_{ij} = 0. \quad (3)$$

The dissipative terms D_{ij} constructed here is based on the work of Jameson [6]. Since the grids are non-deforming, S_{ij} is a constant. Hence Equation (3) becomes

$$\frac{dW}{dt} + R(W) = 0, \quad (4)$$

where $R(W)$ is the residue defined as

$$R_{ij} = \frac{1}{S_{ij}} (Q_{ij} - D_{ij}).$$

Time stepping is done using a four-stage Runge-Kutta scheme with single evaluation of the dissipative terms. This allows a Courant number of $2\sqrt{2}$. A typical k stage scheme is

$$\begin{aligned} W^{(0)} &= W^n, \\ W^{(1)} &= W^{(0)} - \alpha_1 \Delta t R^{(0)}, \\ &\dots \\ W^{(k)} &= W^{(0)} - \alpha_k \Delta t R^{(k-1)}, \\ W^{n+1} &= W^{(k)}. \end{aligned}$$

The maximum time-step allowed in the calculation is found using the eigenvalues of the flux Jacobian matrices as

$$\Delta t = \frac{S_{i,j}}{\max(\lambda_{i+\frac{1}{2},j}, \lambda_{i-\frac{1}{2},j}, \lambda_{i,j+\frac{1}{2}}, \lambda_{i,j-\frac{1}{2}})} \text{CFL}.$$

Here CFL is Courant number and λ_k is the spectral radius on face k defined as

$$\lambda_k = |(u - x_\tau)\Delta y_k - (v - y_\tau)\Delta x_k| + C\sqrt{\Delta x_k^2 + \Delta y_k^2}.$$

The fluid velocity normal to the airfoil is the same as the component of velocity of the moving surface in the normal direction. That is

$$V \cdot \hat{n} = V_n.$$

Three other numerical boundary conditions are imposed by extrapolation from the computational domain onto the solid surface. Assuming that the flow is subsonic at the outer boundary, boundary conditions are imposed using Riemann invariants. The Riemann invariants

$$\begin{aligned} R_\infty &= V_{n_\infty} + \frac{2C_\infty}{\gamma - 1}, \\ R_e &= V_{n_e} - \frac{2C_e}{\gamma - 1}, \end{aligned}$$

correspond to incoming and outgoing waves. The above equations are added and subtracted to give

$$\begin{aligned} V_{n_b} &= \frac{1}{2}(R_\infty + R_e), \\ C_b &= \frac{\gamma - 1}{4}(R_\infty - R_e). \end{aligned}$$

At an outflow boundary the tangential velocity and entropy are specified by extrapolation from the computational domain where-as for an inflow boundary they are the free stream values. These four quantities give a complete definition of the flow in the far field. If the flow is supersonic then all the flow quantities are specified as free stream values at the inflow boundary and are extrapolated at the outflow boundary.

2.2 Aeroelastic solver

The motion of the wing section is described using two degrees of freedom, that is, pitching and heaving. These motions are elastically restrained by two linear springs that model the elasticity of the wing in torsion and bending. The structural parameters of the configuration such as spring stiffness, mass, moment of inertia, and position of the elastic axis, are chosen such that it mimics the motion of the wing section defined by the first two modes of the wing. A flow of uniform velocity is allowed to pass over this airfoil configuration. Due to the airfoil geometry, the Mach number in some regions of flow reaches supersonic speeds leading to shocks. A disturbance to this airfoil can lead to the motion of the shock, which if not in phase with the motion of the airfoil, can lead to energy transfer from the flow to the airfoil leading to flutter.

Since the elastic axis and the center of mass of the airfoil are different for the system, the governing equations are a coupled system of equations. The forcing functions are derived from the flow governing equations. The aeroelastic governing equations of motion are

$$\begin{aligned} m\ddot{h} + S_\alpha \ddot{\alpha} + K_h h &= L, \\ S_\alpha \ddot{h} + I_\alpha \ddot{\alpha} + K_\alpha \alpha &= M_{ea}. \end{aligned}$$

In the above equations h is the heaving degree of freedom of the system, α is the pitching degree of freedom about the elastic axis, K_h is the spring stiffness in heave, K_α is the spring stiffness in pitch, L is the lift on the airfoil, M_{ea} is the aerodynamic moment about the elastic axis, S_α is the static imbalance due to the offset of the mass center from the elastic axis, I_α is the moment of inertia of the airfoil about the elastic axis, and m is the mass per unit span of the airfoil.

Non-dimensionalizing the above equations as

$$\begin{aligned} \tau &= \omega_\alpha t, & x_\alpha &= \frac{S_\alpha}{mb}, & r_\alpha^2 &= \frac{I_\alpha}{mb^2}, \\ \omega_h &= \sqrt{\frac{K_h}{m}}, & \omega_\alpha &= \sqrt{\frac{K_\alpha}{I_\alpha}}, & \mu &= \frac{m}{\pi \rho b^2}, \\ & & k_c &= \frac{\omega_\alpha b}{U_\infty}, \end{aligned}$$

yield

$$[M] \{q\}'' + [K] \{q\} = \{F\}. \quad (5)$$

In the above equation

$$[M] = \begin{bmatrix} 1 & x_\alpha \\ x_\alpha & r_\alpha^2 \end{bmatrix}, \quad [K] = \begin{bmatrix} \left(\frac{\omega_h}{\omega_\alpha}\right)^2 & 0 \\ 0 & r_\alpha^2 \end{bmatrix},$$

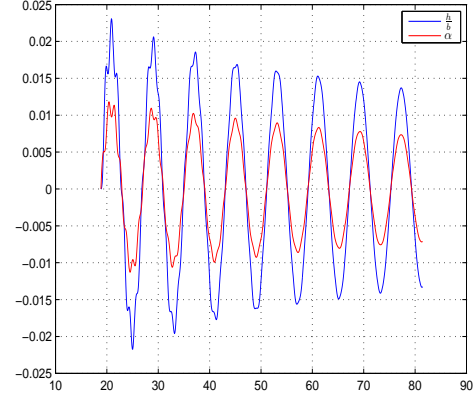
$$[F] = \frac{1}{\pi \mu k_c^2} \begin{bmatrix} C_l \\ 2C_m \end{bmatrix}, \quad \{q\} = \begin{Bmatrix} h \\ \alpha \end{Bmatrix}.$$

In the above, τ is non-dimensional time, x_α is non-dimensional distance between center of mass and elastic axis, r_α is radius of gyration about the elastic axis, ω_h and ω_α are uncoupled natural frequencies of the system in heave and pitch respectively, μ is mass ratio, k_c is reduced frequency, C_l and C_m are coefficients of lift and moment about the elastic axis respectively.

In order to solve Equation (5) the linear acceleration method of time integration is used [10].

3 Results and Discussion

Fig. 1 Damped response for $M=0.85$ and $V_f = 0.439$



3.1 Transonic flutter

Isogai's [2] test case A was considered for the aeroelastic calculations with the following parameters for a NACA64A010 airfoil section

$$x_\alpha = 1.8, r_\alpha^2 = 3.48, \mu = 60, a = -2.0, \frac{\omega_h}{\omega_\alpha} = 1.0.$$

O-grids of size 128×32 extending upto 25 chord-lengths away from the airfoil was used for the study. The airfoil was forced in pitching about the elastic axis at a given Mach number for three cycles at a set frequency of 100 rad/sec and an amplitude 1° . Then the imaginary hinge about which it was pitching was set free, and at the same time the forcing was removed. The evolution in time of the solution was thereafter studied.

The flutter index on the flutter boundary at a given Mach number represents the velocity of the fluid at which the airfoil of unit mass ratio, semi-chord length, and uncoupled natural frequency in pitch, flutters. The frequency at which it flutters is called the flutter frequency. Flutter indices are varied for the given airfoil at each Mach number till a self-sustained neutral response is reached. Flutter boundary is drawn for the given structure. For flutter indices lower than the flutter indices on the flutter boundary a damped response can be observed as in Figure 1. A self-sustained oscillation can be seen as in Figure 2 during flutter. At speeds beyond the flutter speed a diverging re-

Fig. 2 Neutral response for $M=0.825$ and $V_f = 0.612$

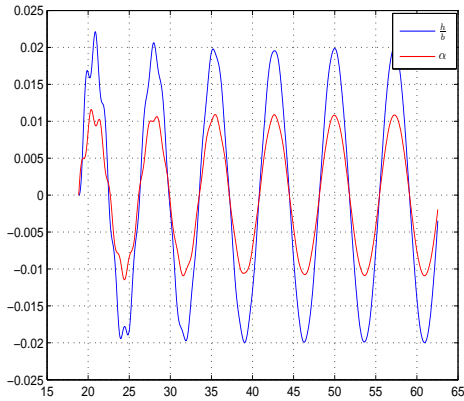


Fig. 5 Limit cycle response for $M=0.75$ and $V_f = 1.320$

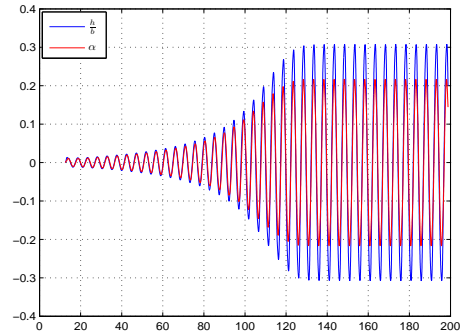


Fig. 3 Divergent response for $M=0.875$ and $V_f = 1.420$

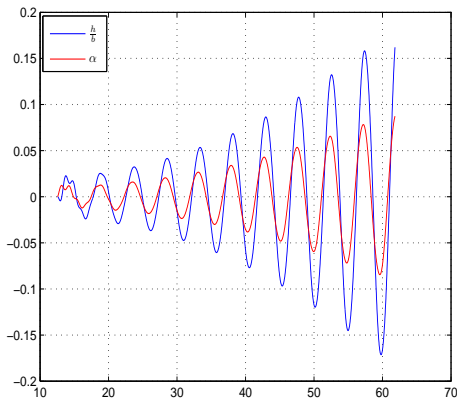


Fig. 6 V_f versus M

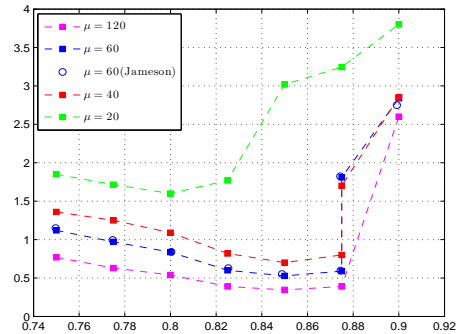
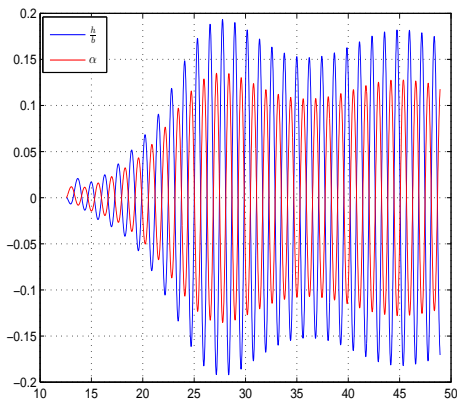


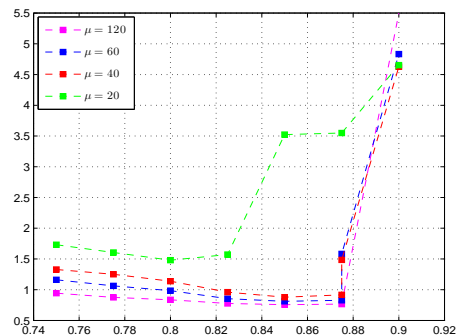
Fig. 4 Second mode response for $M=0.9$ and $V_f = 2.840$



sponse can be observed as shown in Figure 3. In all these cases it can be seen that the response of the aeroelastic system is close to the first mode of the structure. The heave and pitch motion are in-phase. A second mode response of the configuration is shown in Figure 4.

At a given Mach number and beyond the flutter speed the aeroelastic system need not exhibit

Fig. 7 $\frac{\omega_f}{\omega_\alpha}$ versus M



a divergent response for ever. Figure 5 shows the limit cycle response behavior of the system beyond the flutter speed. The amplitude of the response increases initially and later the nonlinearities in the coupled fluid structure problem limit the amplitude of the response.

For the given configuration, at different Mach numbers, the flutter indices and flutter frequencies are determined and graphed as in Figure 6 and 7. These constitute the flutter boundary for the aeroelastic system. Similarly the flutter boundaries are found and shown for different mass ratios on same figures. At a given Mach number multiple flutter points are possible due to the bending back of the flutter boundary. In these figures, we have also shown the results computed by Jameson, *et al.* [6]. Our numerical results are in good agreement with those of [6]. Note that for $\mu = 20$, there is a substantial change in the flutter boundary.

3.2 Shock motion

It is known that the net energy input into the system during flutter is zero, that is, the net energy flow into the airfoil per cycle of oscillation

$$\int_0^T [K] \{q\} \cdot \{q\}' d\tau = \int_0^T [\{F\} - [M] \{q''\}] \cdot \{q\}' d\tau$$

- Net energy > 0 Diverging response
- Net energy < 0 Damped response
- Net energy $= 0$ Neutral response.

In all transonic flow results, the shocks appear on the surface of the airfoil. This is the characteristic of transonic flows. These shocks are called part-chord shocks [3]. When the airfoil oscillates, these part-chord shocks move on the airfoil surface. During transonic flutter when the net energy is zero, we determine the energy contribution by the shock motion into the structure at different locations of the flutter boundary. In order to calculate the energy transfer into the structure due to the shock movement alone, the unsteady air-loads are subtracted from the

steady air-loads in the region between unsteady and steady shocks, and integrated over a cycle of oscillation after multiplying by their respective velocities. That is the work done

$$WD = \int_0^T [\{F_u - F_s\}] \cdot \{q\}' d\tau.$$

Here $\{F_u - F_s\}$ is the force vector acting on the aeroelastic configuration due to the change in pressure distribution in the region between the unsteady and steady shock locations. During one cycle of oscillation of the neutral response, the work done at 20 different time steps are calculated and added to find the work contribution by the shock motion into the aeroelastic system. In order to represent the energy contribution by the shock, this energy is compared with the maximum potential energy of the aeroelastic system. The maximum potential energy is equal to $\frac{[K] \cdot \{q_0\} \cdot \{q_0\}}{2}$. Here $\{q_0\}$ is the vector of amplitude of oscillation of the system during neutral response.

For the case of mass ratio $\mu = 60$, the energy transferred due to shock movement into the structure in the transonic dip regime at $M_\infty = 0.85$ is found to be +0.7159 times the maximum potential energy of the structure. For the same configuration away from the transonic dip regime, at $M_\infty = 0.80$, the energy transfer is found to be +0.0936 times the maximum potential energy of the structure. The above discussion explains the importance of shock and its movement in the transonic dip regime. It is also seen in the dip regime that the frequency of oscillation of the system drops. From Figure 8 it is seen that the amplitude of shock displacement increases drastically with the decrease in reduced frequency hence increasing the importance of the shock in the dip regime. The shock parameters which affect the flutter behavior are the shock strength, shock displacement amplitude which is a function of frequency of oscillation, phase shift between the motion of the shock and the airfoil motion, and also the location of the shock [3].

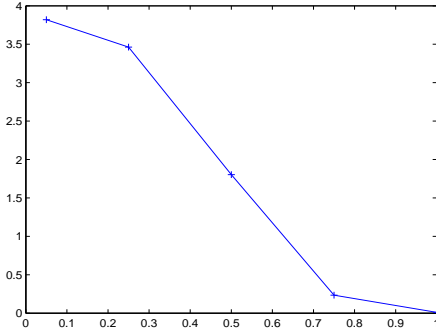


Fig. 8 Shock displacement $\frac{d}{d\alpha}(\frac{x_\alpha}{2b})$ with the variation of reduced frequency in pitching of NACA64A010 airfoil

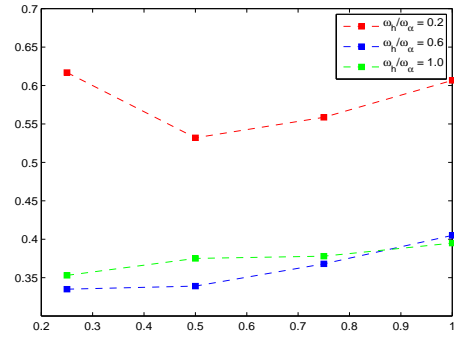
3.3 System parameter effect

The effect of the location of mass center with respect to the elastic axis for different ratios of the uncoupled natural frequencies of the system in heave and pitch on the flutter boundary is shown in Figure 9(a). The airfoil considered for the study is NACA64A010 at $M_\infty = 0.8$ and the elastic axis is fixed at quarter chord. With the increase in the ratio of uncoupled natural frequencies of the system in heave and pitch, the flutter index decreases and with further increase it increases for all values of x_α . A sudden change in the trend of the curves is seen at $x_\alpha = 0.5$ which coincides with the approximate location of the steady shock.

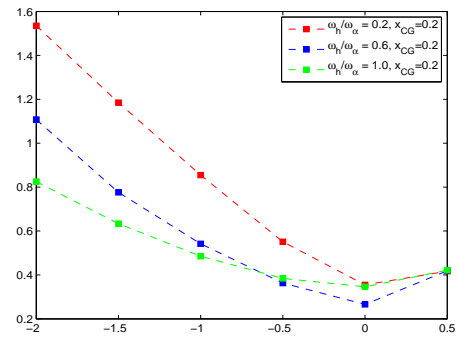
The effect of the location of elastic axis measured with respect to the midchord, on the flutter boundary is shown in Figure 9(b). The center of mass is fixed at $0.2b$ aft of the midchord. The calculations are done on NACA64A010 airfoil at $M_\infty = 0.8$. For the case of the elastic axis aft of the mass center, static divergence occurs before flutter. Figure 10 shows the time response of the system for the above configuration in which the equilibrium point is shifted.

3.4 Viscous effects

Viscous terms are added and discretized using a central difference scheme. A five stage Runge-Kutta scheme is used for time integration. Local

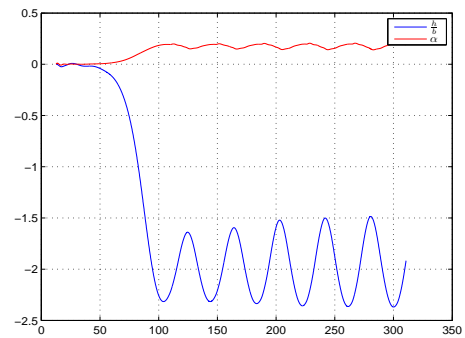


(a) V_f versus x_α keeping elastic axis fixed at quarter chord



(b) V_f versus a keeping mass center fixed at $0.2b$ aft of midchord

Fig. 9 Parameter study - NACA64A010 airfoil, $M_\infty = 0.80$



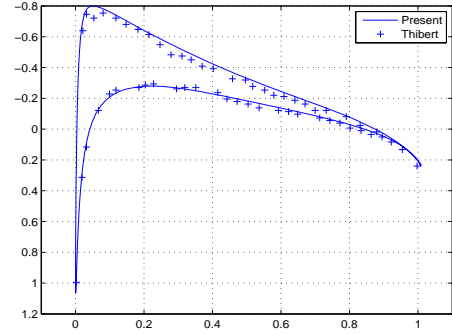
(a) Diverging response at $V_f = 0.417$

Fig. 10 Time response of NACA64A010 airfoil at $M_\infty = 0.80$, $x_\alpha = -0.30$, $a = 0.50$, $\frac{\omega_h}{\omega_\alpha} = 0.20$

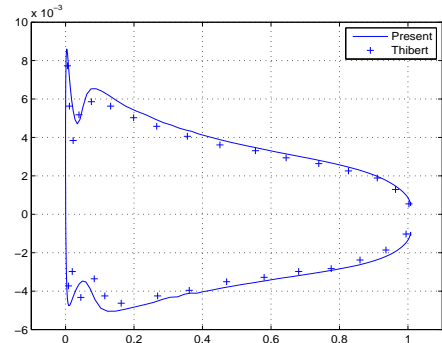
time stepping is used for convergence acceleration. A one equation Spalart-Allmaras [7] turbulence model is used along with density weighted average Navier-Stokes equations to calculate the average flow variables. Two standard test cases are studied and the results are compared with the experimental results. These results are compared with the Euler solution of the same configuration.

Steady turbulent flow over NACA0012 airfoil is simulated when the airfoil is held at an angle of 1.77° to the free stream of Mach number 0.502, Reynolds number 2.91×10^6 defined with respect to its chord, Prandtl number 0.72 and turbulent Prandtl number 0.9. The grids considered for study are C-grids of size 256×72 . The grid spacing on the solid surface is set equal to 3.0×10^{-5} . The far-field is 25 chord-lengths away from the solid surface. Figure 11 shows the pressure distribution, skin friction distribution and residue decay. It has the results computed by an Euler solver for the same configuration. The results are compared with the experimental results of Thibert [8] and are in good agreement with each other. Both Navier-Stokes pressure distribution, Figure 11(a) and Euler pressure distribution, Figure 11(d) are close to the experimental results. A slight variation in pressure distribution on the upper surface of the Euler solution is because of the boundary layer effects whose thickness increases downstream because of the adverse pressure gradient. These results indicate that the inclusion of viscous effects in the subsonic regime at high Reynolds numbers has no significant effect on the calculation of pressure distribution when there are no separation of flow on the airfoil.

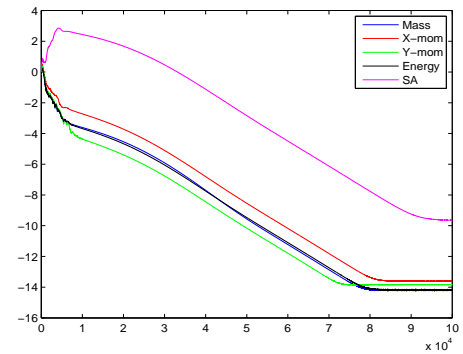
An RAE2822 airfoil is considered for steady turbulent flow analysis. The airfoil is held at 2.79° to the free stream of Mach number 0.73, Reynolds number 6.5×10^6 based on chord length, Prandtl number 0.72 and turbulent Prandtl number 0.9. C-grids of size 256×72 are considered for the study with the grid spacing on the solid surface equal to 1.0×10^{-5} times the airfoil chord. The far-field is 25 chords away from the solid surface. Figure 12 shows the pressure distribution, skin friction distribution, residue decay



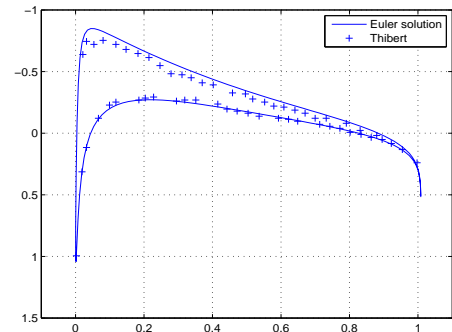
(a) Coefficient of pressure



(b) Coefficient of friction



(c) Residue decay



(d) Euler solution: coefficient of pressure

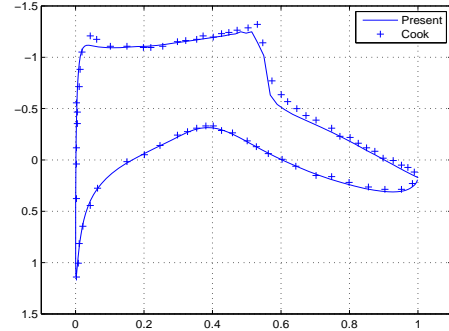
Fig. 11 $M_\infty = 0.502$, $Re_\infty = 2.91 \times 10^6$ at $\alpha = 1.77^\circ$ for NACA0012 airfoil.

of the Navier-Stokes solution. The results from the Euler solver for the same configuration is also shown in the same figure. The results are compared with the experimental results of Cook [9]. The Navier-Stokes results are in good agreement with the experimental results where as the Euler solution differs considerably with the experimental results.

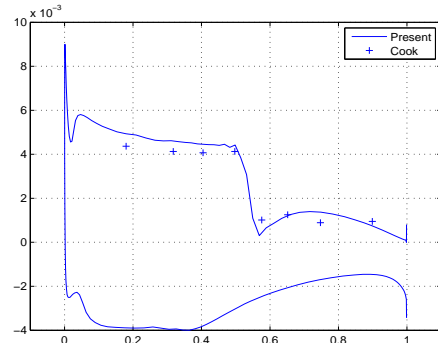
The fluid on the upper surface of the airfoil has reached supersonic regime because of the airfoil geometry. This has led to the generation of the shock. Because of the shock, a sudden jump in the pressure distribution can be seen in the pressure distribution curves i.e., Figure 12(a) and 12(d). The location of the shock has changed drastically in the two solutions, Navier-Stokes solution being close to the experimental results. The boundary layer has a dominant effect in shifting the location of the shock well before the shock location of the Euler solution. The shock strength in the Navier-Stokes solution is less in comparison to the Euler solution. This case establishes the importance of viscous effects in transonic flows.

4 Conclusions

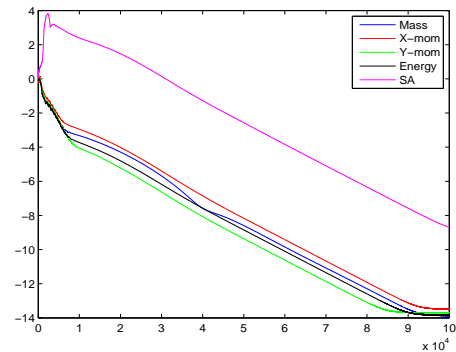
Transonic flow is characterized by the presence of part-chord shocks that demand atleast Euler equations to be solved. Euler equations in integral form are used for flutter calculations using Jameson’s artificial dissipation technique. Single degree of freedom flutter dominates the bottom of the transonic dip. This suggests the energy pumping mechanism is the unsteady shock motion unlike the case of classical bending-torsion flutter. Part-chord shocks and its motion do not allow the amplitude of motion of the airfoil to grow indefinitely. The nonlinear effect of the shock limit the amplitude of oscillation. The limit cycle response is captured by the present code due to the nonlinearities of the aerodynamics. At a given Mach number, multiple flutter points are possible due to the flutter boundary being bent back. Transonic dip is found to be because of the energy transfer into the structure by the shock motions. The energy input into the structure during



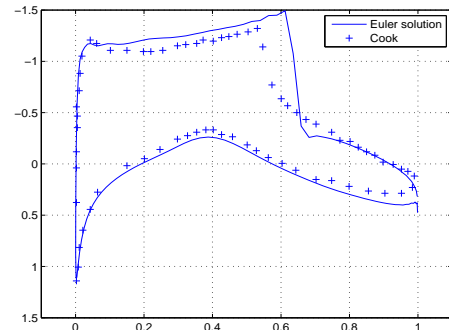
(a) Coefficient of pressure



(b) Coefficient of friction



(c) Residue decay



(d) Euler solution: coefficient of pressure

Fig. 12 $M_\infty = 0.73$, $Re_\infty = 6.5 \times 10^6$ at $\alpha = 2.79^\circ$ for RAE2822 airfoil.

flutter because of the shock motion in the transonic dip region is found to be more than the energy transfer away from the dip region, indicating that compressibility effects are responsible for the transonic dip. The variation of flutter boundary with parameters such as the location of the elastic axis, location of the mass center and the ratio of uncoupled natural frequencies of the system in heave and pitch are presented. A change in the equilibrium position of the system is observed for the case when the elastic axis is aft of the mass center. The amplitude of the shift in equilibrium position suggest that the system has undergone static divergence. Viscosity in the flow results in shifting the shock location and lowering the shock strength.

References

- [1] Y. C. Fung. *An Introduction to the Theory of Aeroelasticity*. John Wiley and Sons, 1957.
- [2] K. Isogai. *On the transonic-dip mechanism of flutter of a sweptback wing*. AIAA Journal, July, 1979, 793-795.
- [3] H. Ashley. *Role of shocks in the sub-transonic flutter phenomenon*. Journal of Aircraft, Vol.17, No.3, 187-197, March, 1980.
- [4] K. Isogai. *Transonic dip mechanism of flutter of a swept back wing: part II*. AIAA Journal, September, 1981, 1240-1242.
- [5] O. O. Bendiksen. *Influence of shocks on transonic flutter of flexible wings*. 50th AIAA/ASME/ASCE/AHS/ASC Structures, Structural Dynamics and Materials Conference, May 2009, AIAA2009-2313, Palm Springs, California.
- [6] A. Jameson, W. Schmidt, and E. Turkel. *Numerical solution of the Euler equations by finite volume methods using Runge-Kutta time-stepping scheme*. AIAA, 14th Fluid and Plasma Dynamic Conference, AIAA 1981-1259, June, 1981.
- [7] P. R. Spalart and S. R. Allmaras. *A one-equation turbulence model for aerodynamic flows*. 30th aerospace sciences meeting and exhibit, AIAA, January 1992, AIAA-92-0439, Reno, NV.
- [8] J. J. Thibert, M. Grandjacques and L. H. Ohman. *NACA0012 airfoil*. AGARD-AR-138, May 1979, Neuilly sur Seine, France.
- [9] P. H. Cook, M. A. McDonald and M. C. P. Firmin. *Airfoil RAE 2822 - Pressure distributions and boundary layer and wake measurements*. AGARD-AR-138, May 1979, Neuilly sur Seine, France.
- [10] G. P. Guruswamy. *Unsteady aerodynamic and aeroelastic calculations for wings using Euler equations*. AIAA Journal, Vol.28, No.3, March 1990, 461-469.

4.1 Copyright Statement

The authors confirm that they, and/or their company or organization, hold copyright on all of the original material included in this paper. The authors also confirm that they have obtained permission, from the copyright holder of any third party material included in this paper, to publish it as part of their paper. The authors confirm that they give permission, or have obtained permission from the copyright holder of this paper, for the publication and distribution of this paper as part of the ICAS2012 proceedings or as individual off-prints from the proceedings.